Korte, M., Constable, C. (2011): Improving geomagnetic field reconstructions for 0–3 ka. - Physics of the Earth and Planetary Interiors, 188, 3-4, 247-259

DOI: 10.1016/j.pepi.2011.06.017

Improving geomagnetic field reconstructions for 0-3 ka

Monika Korte[a], Catherine Constable[b]

[a] *Helmholtz Zentrum Potsdam, Deutsches GeoForschungsZentrum GFZ, Telegrafenberg, 14473 Potsdam, Germany*

[b] *Institute for Geophysics and Planetary Physics, Scripps Institution of Oceanography, University of California, San Diego, 9500 Gilman Drive La Jolla, CA 92093-0225, USA*

Abstract

Global geomagnetic field reconstructions on millennial time scales can be based on comprehensive paleomagnetic data compilations but, especially for older data, these still suffer from limitations in data quality and age controls as well as poor temporal and spatial coverage. Here we present updated global models for the time interval 0–3 ka where additions to the data basis mainly impact the South-East Asian, Alaskan, and Siberian regions. We summarize recent progress in millennial scale modelling, documenting the cumulative results from incremental modifications to the standard algorithms used to produce regularized time-varying spherical harmonic models spanning 1000 BC to 1990 AD: from 1590-1990 AD gauss coefficients from the historical *gufm1* model supplement the paleomagnetic information; in addition to absolute paleointensities, calibrated relative paleointensity data from sediments are now routinely included; iterative data rejection and recalibration of relative intensity records from sediments ensure stable results; bootstrap experiments to generate uncertainty estimates for the model take account of uncertainties in both age and magnetic elements and additionally assess the impact of sampling in both time and space. Based on averaged results from bootstrap experiments, taking account of data and age uncertain- ties, we distinguish more conservative model estimates *CALS3k.nb* representing robust field structure at the core-mantle boundary from relatively high resolution models *CALS3k.n* for model versions n =3 and 4. We assess the impact of newly available data and modifications to the modelling method by comparing the previous *CALS3k.3*, the new *CALS3k.4*, and the conservative new model, *CALS3k.4b*. We conclude that with presently available data it is not feasible to produce a model that is equally suitable for relatively high-resolution field predictions at Earth's surface and robust reconstruction of field evolution, avoiding spurious structure, at the core-mantle boundary (CMB). We presently consider *CALS3k.4* the best high resolution model and recommend the more conservative lower resolution version for studies of field evolution at the CMB.

Key words: Geomagnetism, field model, archaeomagnetic field, millennial secular variation.

1. Introduction

Geomagnetic field changes are rather well documented since the advent of routine direct measurements several centuries ago, but this time frame is not sufficient for the larger goal of understanding the physical processes that control long term changes in the geodynamo in Earth's core. Significant efforts have been made over recent years to reconstruct not only the axial dipole strength, but also the dipole tilt and further large scale regional field variations on millennial timescales (Johnson and Constable, 1998; Hongre et al., 1998; Constable et al., 2000; Korte and Constable, 2003, 2005; Valet et al., 2008; Korte et al., 2009; Nilsson et al., 2010). Global compilations from numerous publications of archeomagnetic data (Donadini et al., 2006; Genevey et al., 2008; Donadini et al., 2009) and paleomagnetic records from sediments with high accumulation rates (Korte et al., 2005; Korte and Constable, 2006; Donadini et al., 2009) are the basis for such global field models. The spherical harmonic models, *CALS3K.1* (Korte and Constable, 2003) and *CALS7K.2* (Korte and Constable, 2005), with the names standing for "Continuous model from Archeomagnetic and Lake Sediment data of the past 3/7 kyrs", have been used in a broad suite of applications. These range across investigations of westward and eastward motions in the core (e.g. Dumberry and Bloxham, 2006; Dumberry and Finlay, 2007; Wardinski and Korte, 2008), field asymmetry related to archeomagnetic jerks (Gallet et al., 2009), geomagnetic shielding for cosmic rays and cosmogenic isotope production for various kinds of studies (e.g. Usoskin et al., 2006; Muscheler et al., 2007; Usoskin et al., 2008; Lifton et al., 2008), to data assimilation for geodynamo models (Kuang et al., 2008). Despite these successes, previous attempts to characterize the spatial and temporal resolution of these models (Korte and Constable, 2008) have highlighted a number of issues with the available data and limitations of the chosen modelling techniques that lead to significant uncertainties in millennial scale geomagnetic field reconstructions.

Archeomagnetic data in general have smaller experimental uncertainties than those derived from sediments and their dating is often more precise. However, the number of archeomagnetic results available for times prior to 1000 BC is too small to allow for global reconstructions based purely on this data type. Even for the most recent epochs such information comes mostly from the northern hemisphere, and particularly from Europe, resulting in regionally biased models from these limited sources (Korte et al., 2009). Sediment records have a better geographic distribution, and are thus essential for global modeling efforts, but they are also intrinsically noisier. In some cases depositional and post-depositional processes will smooth out rapid field variations and they may suffer from strong dating uncertainties related to magnetization lock-in depth or radiocarbon reservoir effects that can influence large parts of or even complete time series. Moreover, intensity variations obtained from sediments are only relative, and must be calibrated somehow for use in global geomagnetic modeling. In recent work, Donadini et al. (2009) and Korte et al. (2009) constructed a suite of models using various classes of data and were able to show that even those based exclusively on sedimentary records, comprising magnetic field directions and suitably calibrated intensities, provide reasonable if somewhat smoothed reconstruction of past field variations. It should, however, be noted that some of the contributing records appear inconsistent with one another so that individual data records may have a poor fit to the resulting model. For regional studies, it makes sense to consider only highest quality data which can provide more detailed information for a specific geographical area than is possible with a global model. For the global field evolution, however, Korte et al. (2009) concluded that the best reconstructions were produced using a combination of all available information, including knowledge derived from direct field observations spanning the interval 1590-1990 AD.

In this work we investigate the influence of modifications to the modelling method and the data by comparing two new models spanning the past 3 kyrs to the immediate predecessor *CALS3k.3* (Korte et al., 2009). Section 2 details some additions to our data set. Then we summarize the evolution of the basic modeling method and describe improvements regarding outlier rejection, calibration of relative intensity data and obtaining a more conservative model by a bootstrap average. We discuss aspects of robustness and sensitivity of the *CALSxk* type models to changes in modelling and to the addition of newly available data by comparing *CALS3k.3*, the new *CALS3k.4* and the more conservative new model, *CALS3k.4b*.

2. An Updated Data Set

The data set used here is based on and extended from earlier compilations by Korte et al. (2005); Genevey et al. (2008); Donadini et al. (2009). These span the time interval 10000 BC to 1990 AD to allow for a future 10 or 12 kyr model. The archeomagnetic data consist of all those included in the GEOMAGIA V.2 database (Korhonen et al. (2008); Donadini et al. (2009), https://geomagia.ucsd.edu/) by August 2009. There are 163 more archeomagnetic data than were used for *CALS3k.3*, consisting of 56 declination, 57 inclination and 50 intensity values.

The greatest changes are in the sedimentary data compilation which consists of the records compiled as SED3k_dat0 for the past 3 kyrs by Donadini et al. (2009) (see their table 4), plus new records from 13 additional locations, summarized in table 1 and shown in Fig. 1. The previous record from Lake Biwa (Ali et al., 1999) spanning less than 10 kyr has been replaced by more recently published results by Hayashida et al. (2007) from the same lake. The numbers of data are listed in table 2. There are almost 4800 more data than were available for the previous model, *CALS3k.3*.

Table 1: Newly compiled lake sediments.

Abb.	Name	Region/Country	Reference	Lat.	Long.	Age Range	Nr. of data (D/I/F)	Dating
AAM	Alaskan margin	Arctic Sea	Lisé-Pronovost et al. (2009)	71.63	-156.86	6010 BC - 172 AD	994/994/994	C14
BEA	Beaufort sea	Arctic Ocean	Barletta et al. (2008)	70.63	-135.88	2629 BC - 1556 AD	561/556/561	C14
BI2	Lake Biwa	Japan	Hayashida et al. (2007)	35.25	136.06	37681 BC - 112 BC	141/141/137	C14
CHU	Chukchi Sea	Arctic Ocean	Barletta et al. (2008)	72.86	-158.87	7561 BC - 336 AD	1070/1070/1070	C14
EIF	Eifel maars	Germany	Stockhausen (1998)	50.12	6.83	11050 BC - 1850 AD	234/234/0	varves
ERH	Erhai Lake	China	Hyodo et al. (1999)	25.82	100.17	4664 BC - 1922 AD	134/134/0	C14
ERL	Erlongwan Lake	China	Frank (2007)	42.3	126.37	36050 BC - 550 AD	106/106/0	C14
FIN	2 Finnish Lakes	Finland	Haltia-Hovi et al. (2010)	63.62	29.02	7950 BD - 1970 AD	993/993/0	varves
LOU	Louis Lake	Wyoming, USA	Geiss et al. (2007)	42.6	-108.85	17433 BC - 1471 AD	38/36/0	C14
SAG	Saguenay Fjord	Canada	St-Onge et al. (2004)	48.30	-70.26	5214 BC - 1799 AD	1095/1114/0	C14
SAN	Hoya de San Nicolas	Mexico	Chaparro et al. (2008)	20.39	-101.26	9730 BC - 860 BC	176/176/0	C14
SCL	Lake Shuangchiling	China	Yang et al. (2009)	19.94	110.19	6981 BC - 1747 AD	637/647/0	C14
WA1	PS69/274-1	West Amundsen Sea	Hillenbrand et al. (2009)	-73.86	-117.76	22593 BC - 775 AD	0/0/19	C14
WA2	PS69/275-1	West Amundsen Sea	Hillenbrand et al. (2009)	-73.89	-117.55	13207 BC - 1526 AD	0/0/33	C14
WA3	VC424	West Amundsen Sea	Hillenbrand et al. (2009)	-73.45	-115.2	17427 BC - 1129 AD	0/0/34	C14
WPA	West Pacific	West Pacific	Richter et al. (2006)	24.8	122.5	7473 BC - 1934 AD	0/3351/3387	C14

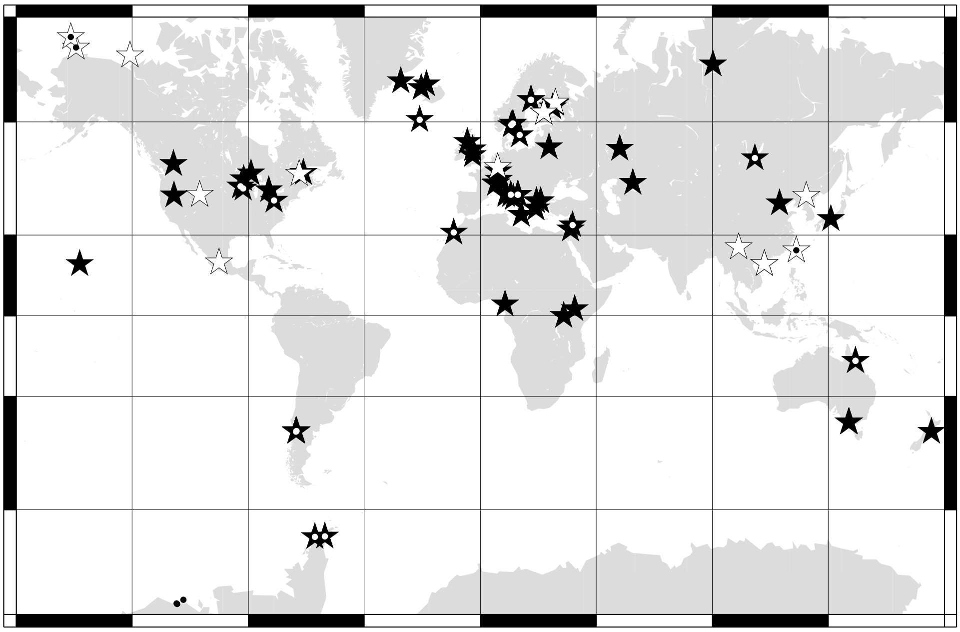

Figure 1: Locations of lake sediment records. Black stars indicate directional and white dots intensity records used in *CALS3k.3*. White stars indicate directional and black dots intensity records for the newly compiled records listed in Table 1.

Recently published sedimentary records dated by ^{14}C are usually calibrated to calendar ages and can be added directly to the global compilation. For older publications with uncalibrated records the calibration procedure is described in detail by Donadini et al. (2009). Sediment declination records were checked for correct orientation by comparing with predictions from the *CALS3k.3* model (Korte et al., 2009). The only case where cores were obviously unoriented was the Chukchi Sea data of Barletta et al. (2008). This record was adjusted by +126° to agree on average for the past 3kyrs with the *CALS3k.3* predictions. Similarly, inclination records were compared with *CALS3k.3* to check for systematic deviations such as inclination flattening. No obvious anomalies were found. Sedimentary relative intensity records were initially calibrated by scaling them against predictions from *CALS3k.3* as a first guess model as described in detail by Korte and Constable (2006) and later applied by Korte et al. (2009). Note that the orientation check and in one case adjustment and the calibration by means of the *CALS3k.3* model may

Table 2: Numbers of data in time interval 1000 BC to 1990 AD.

	before outlier rejection			final		
	Archeomag.	Sediment	All	Archeomag.	Sediment	All
Declination	2814	10016	12830	2801	9669	12470
Inclination	4228	11542	15770	4139	11033	15172
Intensity	2719	4458	7177	2517	4202	6719
All	9761	26016	35777	9457	24904	34361

introduce some dependence of the new model version on the old one. This should not pose a problem when we try to improve a reasonable model, but might have a somewhat limiting effect on differences of average dipole magnitude and field predictions in the Alaskan region in our comparison of models.

The data are weighted according to their uncertainty estimates in the modeling, therefore consistent error estimates are important. We have used the same scheme as was applied to the data set for *CALS3k.3* and provide a brief summary here. Based on the average deviation of archeomagnetic data between 1590 and 1990 and the historical *gufm1* model (Jackson et al., 2000), α_{95} for archeomagnetic directional data was assigned a minimum value of 4.3° if no uncertainty estimates were originally given or the values were smaller and therefore considered unrealistic. The α_{95} or other forms of uncertainties (usually 1 standard errors) were converted to standard deviations of declination and inclination as described by Donadini et al. (2009) For sedimentary directional data, the average deviation from the historical model is larger, although the statistics are less reliable because of the lack of very recent sediment data. The minimum α_{95} uncertainty was set to 6.0° for sediments. In practice, however, very few sedimentary records come with uncertainty estimates and thus nearly all sedimentary records are weighted equally in the end. For intensity data, the minimum uncertainty (standard error) was set to 5μT for both data types, again based on the average deviation between the archeomagnetic intensity data and *gufm1*. No minimum value was used for age uncertainties, as some archeomagnetic artefacts or lavas from historical times can be dated very exactly. However, if no age uncertainties were originally given, they were set to 100 years for archeomagnetic data. Age uncertainties are at present not considered in our individual models and sediment age uncertainties were all fixed to one value in the bootstrap method described below.

3. The modeling method

The regularized modeling method using an expansion in spherical harmonic basis functions in space and cubic B-splines in time is essentially the same as for our earlier models and has been described in detail elsewhere (Bloxham and Jackson, 1992; Jackson et al., 2000; Korte and Constable, 2003, 2008). The spherical harmonic basis is expanded to degree 10 and the knot-point spacing of the splines is chosen as 10 years here. The actual spatial and temporal resolution after regularized inversion that is feasible depends on the data quality, distribution, and uncertainties and is expected to be about spherical harmonic degree 4 and roughly 100 years, see Korte and Constable (2008). The factors governing the strength of the spatial and temporal regularization of the preferred model were chosen by visual comparison of the geomagnetic power spectra of the main field and secular variation to those of the historical model *gufm1* (Jackson et al., 2000) and the International Geomagnetic Reference Field (IGRF 10^{th} generation for 2005, (Maus et al., 2005)) in the same way as for *CALS3k.3* and the other models described by Korte et al. (2009). The main regularization parameters used are the same as for *CALS3k.3* and are given in table 4 for comparison to previous models.

For the recent *CALS3k.3* model, we adopted the strategy of penalizing departures from the *gufm1* model for the time intervals 1840–1990 AD and 1650–1990 AD for the axial dipole and higher degree and order coefficients, respectively (Korte et al., 2009). As for the general spatial and temporal complexity, the strength of this constraint on the coefficients is determined by a Lagrange multiplier, and we have learned from experience that the outcome must be carefully monitored. We now believe that the value of the Lagrange multiplier used for *CALS3k.3* was too small, resulting in significant departures from *gufm1* at the regional level. Although there is good agreement of the first few *CALS3k.3* model coefficients with those from *gufm1* we failed to notice that unreliable data from the top of the Lake Pepin record (Brachfeld and Banerjee, 2000) have an influence on the local model predictions for North America from about 1870 AD onward. For *CALS3k.4*, we have chosen a stronger multiplier (see table 4) which ensures agreement of constrained coefficients to within 1% up to at least degree 8, that is to significantly higher degrees than we can generally resolve with the archeo- and paleomagnetic data. Note that in this way we can cover the whole 3kyr time interval with one model that provides a good description of the field evolution during historical times. Any incompatibilities that might cause a mismatch between the millennial-scale and historical models (Lodge and Holme, 2008) are smoothed out around the 16^{th} to 17^{th} century AD. To minimize the impact of spline end constraints in the early part of the model, the time interval is extended to 2000 BC, but we claim validity only from 1000 BC forward.

In an improvement on our earlier modeling strategy, we used several phases of outlier rejection and re-calibration of relative intensities. Thus a model is now built iteratively in several stages:

- *Step A.* A first guess model A is constructed based on the initial dataset with relative sediment intensities calibrated by model *CALS3k.3*.

- *Step B.* An analysis of residuals is carried out for Model *A* and observations lying outside the 99% confidence interval are rejected as outliers, as in the construction of *CALS3k.3* (see Donadini et al. (2009)). A new model, *B1*, is created from the outlier-free data set.

- *Step C.* The sediment relative intensity records (after outlier rejection) are re-calibrated by Model *B1*. A third model, *C1*, is generated using the new data set with the re-calibrated data.

Steps *B* and *C* are repeated. Calibration factors for some of the records change by as much as 20% in the first iteration, but the average for all records is 5%. By the third iteration there is very little further change: on average the factors change by 0.6% with the largest changes amounting to 2% in two cases. By stage *B3* we have reached our final model. The number of outliers rejected between the original and final data sets amounts to 4% on average, with the smallest percentage for archeomagnetic declination data and the largest for sedimentary intensities. Numbers for the initial and final data set are given in Table 2.

Estimates of model uncertainties were obtained using the combined magnetic values and age (MA) and spatial and temporal distribution (ST) bootstrap method described in detail in Korte et al. (2009) and called the MAST method there. This method takes account of the age and other uncertainties of the final data set as well as the data distribution. For each of the 2000 bootstrap samples we create data sets by drawing on the data set used in building the final version of the corresponding individual model. The bootstrap models are then derived directly without further iterative recalibration or rejection of data. The simulated data at each location are generated in two steps with slight differences for archeomagnetic and sediment data due to their different characteristics. (1) For archeomagnetic data the first is an independent sampling from two normal distributions: one is centered on the value of the magnetic element with a standard deviation corresponding to the uncertainty estimate assigned for our modeling purposes and the other is centered on the age estimate, and uses its respective standard error. For sediment records, the sampling for each datum from a normal distribution centered on the magnetic element is done in the same way, but for the temporal sampling each complete time series is shifted by a value taken uniformly distributed from a time interval of +/- 300 yrs around the original ages in order to preserve the stratigraphic chronology. This introduces strongly correlated samples in the bootstrap. Note that while a truly statistical bootstrap of independent samples should capture any realistic fast variation in the data, this treatment of sediment records is likely to smooth out existing temporal variation. However, in the absence of detailed information about tie points used in constructing the chronology this is a reasonable approach. (2) Bootstraps are performed on these data sets, where for the archeomagnetic data the number of data locations is fixed and values are picked by uniform random sampling from that data set. For the sediments, the number of records is fixed and the locations are again uniformly sampled.

To obtain a high resolution model we previously used the final model from the original data set (after outlier rejection) as our preferred model for *CALS3k.3*. Here, we present two new models.

- *CALS3k.4* is equivalent to *CALS3k.3* but uses the expanded data set along with the iterative data rejection and re-calibration of the sediment intensities. The two models have similar resolution. A comparison allows us to investigate the robustness of detailed spatial and temporal structure under minor improvements to the modelling technique and focussed additions of new data. The number of new data added might be regarded as typical for an updated model version and highlights the impact to be expected for improved geographical coverage.

- *CALS3k.4b* is produced by averaging the 2000 individual MAST bootstrap models. This is a more conservative field reconstruction maintaining only the most robust spatial and temporal features with lower temporal and spatial resolution. This can be useful for studies of field evolution at the core-mantle boundary, where small-scale features including noise become enhanced compared to Earth's surface by the downward continuation.

For comparison, we also created *CALS3k.3b* from the average of the 2000 bootstrap models drawn from the data set used for *CALS3k.3*. Table 3 summarizes our past and new *CALSxk* models with the most significant differences in modelling technique and data basis and our usage recommendations. The new models are available at http://earthref.org/erda/1142 together with Fortran codes that allow users to obtain model predictions with uncertainty estimates from them. Dipole moment predictions from all four models with MAST bootstrap uncertainties for the averaged versions are provided as supplemental material.

Table 3: Overview over *CALSxk* type models

Model	Reference	Time interval	Nr. of data archeo/sediment/all	Improvements in modelling	Recommendation
ALS3K	Constable et al. (2000)	1000 BC to 1800 AD	500 directional smoothed curves	100 yr snapshots; regularization axial dipole evolution prescribed	outdated
CALS3K.1	Korte and Constable (2003)	1000 BC to 1950 AD	as above	continuous	outdated
CALS3K.2	Korte and Constable (2005)	1000 BC to 1950 AD	all 19376	individual data with iterative outlier rejection; archeointensity data included; ax. dipole also from data	outdated
CAKS7K.2	Korte and Constable (2005)	5000 BC to 1950 AD	9400/22953/32353	as above	known shortcomings will be superseded by *CALS10k.1b*
CALS3k.3	Korte et al. (2009)	1000 BC to 1990 AD	9605/20375/29980	weak agreement with *gufm1*; calib. rel. intensity included	superseded by *CALS3k.4*
ARCH3k.1	Korte et al. (2009)	1000 BC to 1990 AD	9605/–/9605	as above	only N hemisphere Earth surface studies
SED3k.1	Korte et al. (2009)	1000 BC to 1990 AD	–/20375/20375	as above	outdated
CALS3k.4	this study	1000 BC to 1990 AD	9761/26016/35777	strong agreement with *gufm1*; iterative re-calibration of rel. intensities;	best for Earth surface studies
CALS3k.4b	this study	1000 BC to 1990 AD	as above	as above; bootstrap average	for CMB studies
CALS10k.1b	manuscript in prep.	8000 BC to 1990 AD	all 86996	as for *CALS3k.4b*	best for long-term CMB studies

4. Results

An overview of the models and their parameters is given in Table 4 and Fig. 2, where using the terminology of all our previous models λ and τ are the spatial and temporal regularization factors, respectively. The value of the spatial norm, Ψ, is the lower bound of the integrated Ohmic dissipation of the field over the Earth (Gubbins, 1975) and a measure of spatial complexity. The temporal variability is measured by temporal norm Φ, the integral of the second derivative of the radial field component over the Earth. The high value of "gufm constraint" compared to the *CALS3k.3* model ensures agreement between the new models and *gufm1* even for smaller scale details. However, this leads to a strong increase in spatial and particularly temporal complexity of the model from 1640 to 1990 AD (see Fig. 2). The significantly higher temporal norm values for *CALS3k.4(b)* compared to *CALS3k.3(b)* mostly result from that modification. The root mean square misfit values given for the bootstrap average models are based on the original dataset on which the bootstraps were performed, i.e. on the same dataset that the respective non-averaged model is based on. These values are essentially identical to those obtained by averaging the rms misfits of each bootstrap model to its own bootstrap dataset, although we observe both better and worse fits in these individual cases (by up to 15% in terms of rms misfit). The *CALS3k.3* and *CALS3k.4* models clearly have smaller rms misfits than their respective bootstrap averages. It is still difficult to assess how realistic and internally consistent our error estimates on the dataset are overall. The increase of average misfit of the bootstrap models indicates less internal consistency of the bootstrap datasets on average, suggesting that the ranges of variation in our MAST bootstrap may be too large rather than too small. However, this might be mostly due to the treatment of the sedimentary records in the bootstrap. The fact that even for the individual models the data cannot be fit within the error estimates by physically reasonable models, i.e. models showing fewer small-scale features than models based on much more accurate direct observations, might suggest that the individual error estimates could be too small. In this case, however, it must also be kept in mind that age uncertainties are not considered in the uncertainty estimates used for weighting the data in the individual models and consequently we should not expect a fit to a normalised rms misfit of 1.0. It is also not obvious why the fit to declination is consistently worse than to the other component data.

Figure 2 clearly shows the smoothing effect of the bootstrap averaging in space and an even stronger effect in time. Only the most robust features of the different models are preserved in the averages. The comparison of main field and secular variation power spectra in Fig. 3 reveals that the smoothing effect of the bootstrap averaging affects all coefficients except for the dipole strength, not just the high spherical harmonic degrees. The slightly greater power in higher degree main field coefficients and the clear increase in small-scale temporal variability in the time-averaged spectra of the version 4 models are mostly caused by the strong influence of the high-resolution *gufm1* model at the end.

The temporal variation of dipole moment and dipole tilt (Figs. 4 and 5) are significantly damped by applying the bootstrap average, while several of the shorter-term variations appear reasonably robust in the comparison between *CALS3k.3* and *CALS3k.4*. Two

Table 4: Model parameters with nomenclature as used for previous models for comparison.

Model	*CALS3k.3*	*CALS3k.3b*	*CALS3k.4*	*CALS3k.4b*
spatial factor $\lambda(\mathrm{nT}^{-2})$	2×10^{-13}	(2×10^{-13})	2×10^{-13}	(2×10^{-13})
spatial norm $\Psi(\mathrm{nT}^2)$	172×10^{11}	149×10^{11}	177×10^{11}	144×10^{11}
temp. factor $\tau(\mathrm{nT}^{-2}\mathrm{yr}^4)$	2×10^{-3}	(2×10^{-3})	2×10^{-3}	(2×10^{-3})
temp. norm $\Phi(\mathrm{nT}^2\mathrm{yr}^{-4})$	243	42	827	583
$gufm$ constraint	1×10^{-2}	1×10^{-2}	1×10^{2}	1×10^{2}
normalized rms				
misfit all data	1.83	1.95	1.68	1.84
rms declination	2.07	2.14	1.90	2.02
rms inclination	1.71	1.78	1.62	1.78
rms intensity	1.78	1.92	1.36	1.62
remarks	-	average of 2000 bootstraps	3 iterations of outlier rejection and recalibration	average of 2000 bootstraps

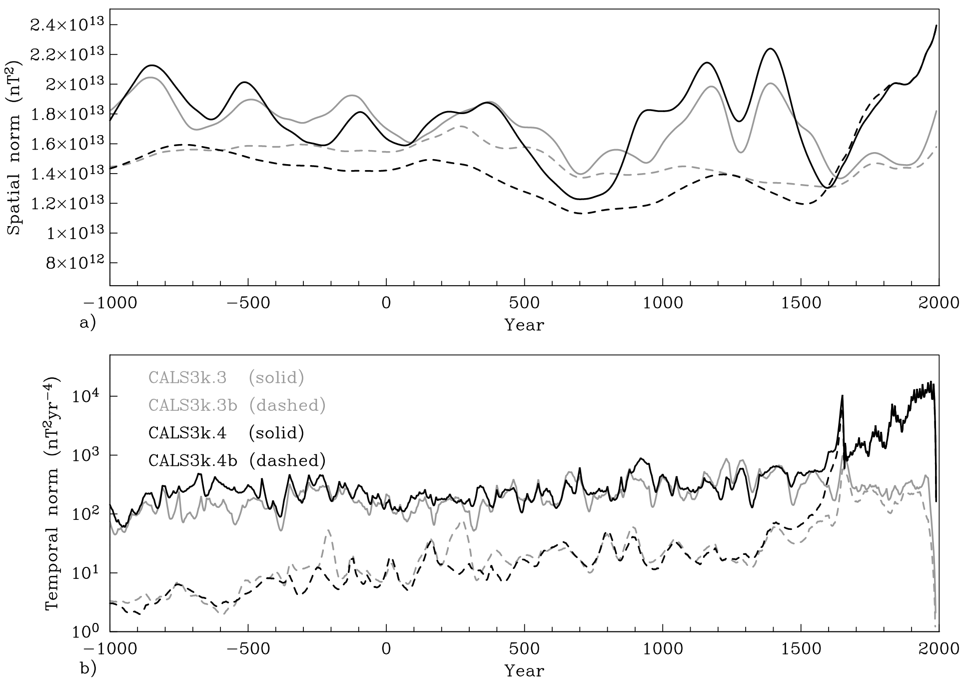

Figure 2: Spatial (a) and temporal (b) norms with time as a measure of complexity of models *CALS3k.3* (gray solid line), *CALS3k.3b* (gray dashed line), *CALS3k.4* (black solid line) and *CALS3k.4b* (black dashed line). Note the logarithmic scale used for the temporal norm.

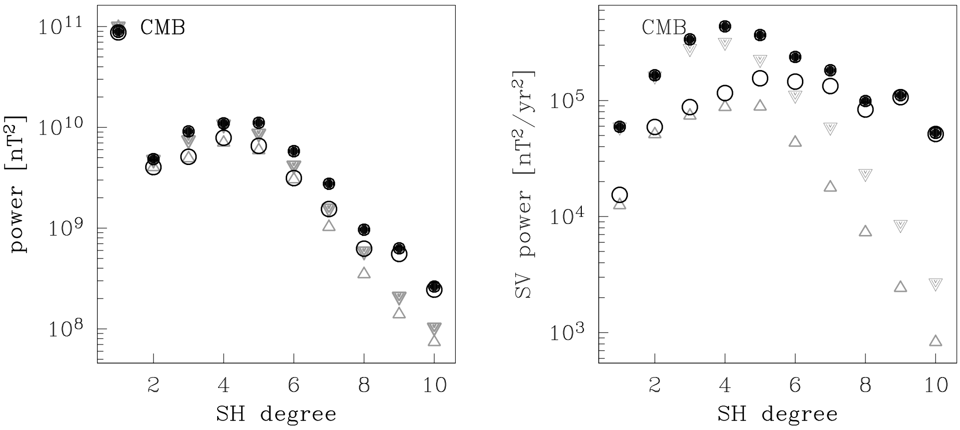

Figure 3: Geomagnetic main field (left) and secular variation (right) power spectra for the models *CALS3k.3* (gray filled triangles), *CALS3k.3b* gray open triangles, *CALS3k.4* (black dots) and *CALS3k.4b* (black circles).

results are somewhat surprising: Firstly, the dipole moment of the version 4 models is lower by about 6% than that of the version 3 models. Secondly, *CALS3k.4* shows stronger tilt of the dipole than *CALS3k.3* at about 600 BC and 1000 AD.

The stronger dipole tilts appear generally consistent in direction, but higher in amplitude than the signals in*CALS3k.3*. Moreover, they seem rather consistent with the dipole tilt models obtained by averaging virtual geomagnetic pole data from archeomagnetic data (Valet et al., 2008) and from five globally well-distributed sediment records chosen for high quality data and named *DE-FNBKE* by Nilsson et al. (2010). These comparisons suggest that the additional data in *CALS3k.4* consistently confirm trends exhibited across our global dataset. The longitudinal movement of the dipole axis predicted by all four models is quite uniform. The unusual eastward swing apparent in *CALS3k.3* between 100 BC and the BC/AD transition occurs at a time when the geomagnetic axis nearly coincides with the geographic axis and very small dislocations can appear as large variations in longitude. The only significant difference in dipole axis longitude occurs between 1000 and 1600 AD, when *CALS3k.4* predicts a westward swing while the other models, including *CALS3k.4b*, predict an eastward swing.

To illustrate regional differences among the models we first present two examples of model predictions in Fig. 6. The data from Lake Frangsjön (Snowball and Sandgren, 2002; Snowball et al., 2007) in Sweden (panel a) were included in the version 3 models. All models are very consistent in their predictions for the directional data with slightly more variation in the individual models than the bootstrap averages. Small differences between the version 3 and version 4 models occur in intensity predictions, where the data in general are not fit very closely by the models. The data from Lake Shuangchiling (Yang et al., 2009) in China are a new addition to the data compilation along with two other records from the same general region. Again the data are not very well fit by any of the models. Clear differences among the individual models appear in all components, but the differences among the models are relatively modest in comparison with the data misfit. The bootstrap

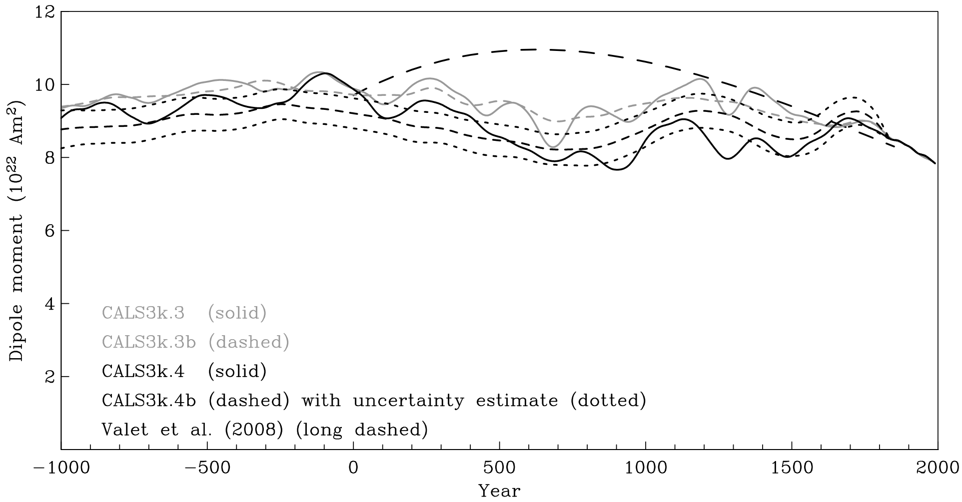

Figure 4: Dipole moment of models *CAlS3k.3* (gray solid line), *CALS3k.3b* (gray dashed line), *CALS3k.4* (black solid line) and *CALS3k.4b* (black dashed line). One standard deviation uncertainty estimates from the bootstrap are shown (dotted lines) for CALS3k.4b and lie in the same order for the other models. The virtual axial dipole moment reconstruction by Valet et al. (2008) (long dashed line) is also included.

model predictions are in reasonable agreement with each other for the directional data for nearly all of the time, smoothing out much of the stronger variation seen particularly in *CALS3k.4*. These results are quite representative of the regional differences and are not surprising: In regions and at times where data were available for the version 3 models the version 4 models in general differ very little, whereas in regions where new data have been included and partly in regions that still suffer sparse data coverage more significant differences occur. Interested readers can find plots analogous plots to Figure 6 for all the sediment records online at http://earthref.org/erda/1143.

The relatively poor fit to observations exhibited in Figure 6 might be regarded as a significant cause for concern, and is certainly an indication that one should be cautious about over-interpreting the model results. However, it should be borne in mind that the observations at Earth's surface represent an integrated view of fields upward continued from the core-mantle boundary (CMB), and can be influenced by changes at the CMB at large geographic distances (Constable (2007), Figure 13). Regional incompatibilities in the observations at Earth's surface can extend to broad spatial scales as a result so that while the model reflects the need to fit all the relevant data it is not always obvious why a specific data set has large deviations from model predictions.

We turn now to predictions of the radial field component, $B_r(c)$, at the core-mantle boundary (CMB) which are of interest for studying geodynamo processes. In interpreting the results it is again important to be aware of the spatial coverage of the CMB provided by the observations. Constable et al. (1993) describe how the magnetic field at Earth's surface can be written in terms of the Green's function for the radial magnetic field, $B_r(c)$. For paleomagnetic observations of declination, inclination, and intensity, the relationship to $B_r(c)$ is non-linear, but linearized data kernels describe how these observations respond

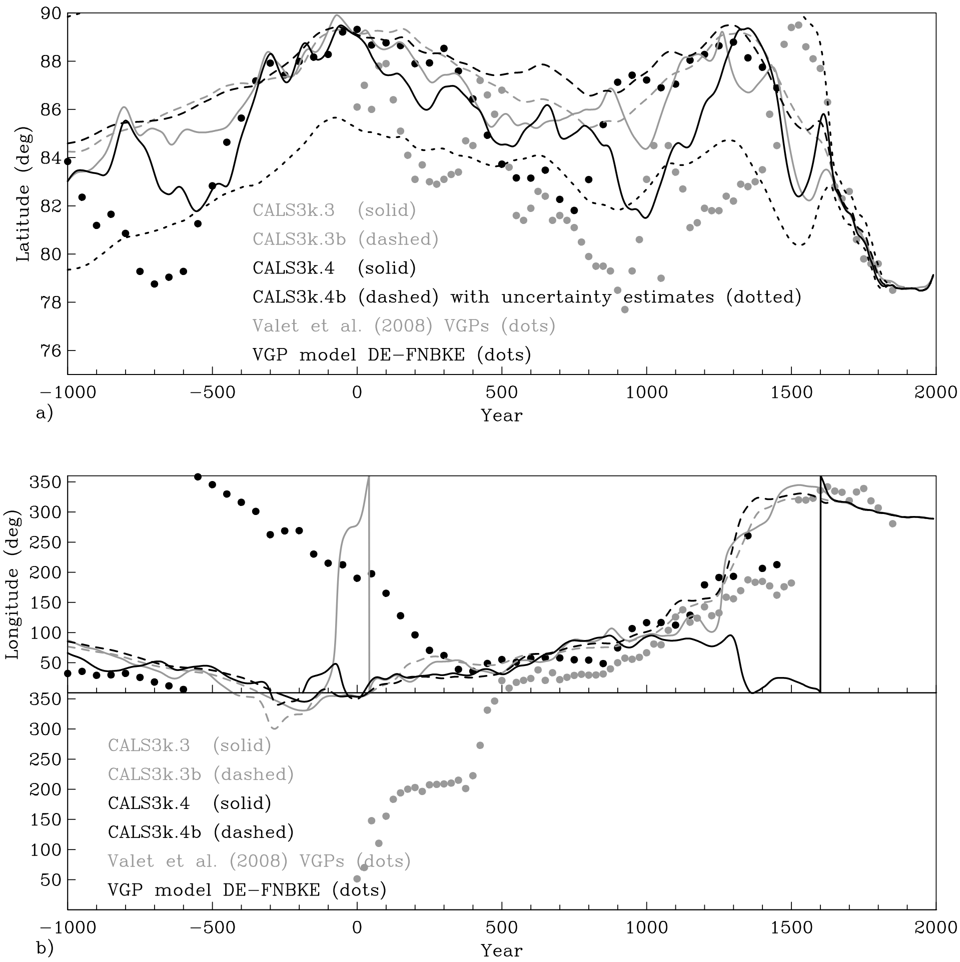

Figure 5: Evolution of the dipole axis in latitude (a) and longitude (b) of the geomagnetic pole as predicted by the models *CAlS3k.3* (gray solid line), *CALS3k.3b* (gray dashed line), *CALS3k.4* (black solid line) and *CALS3k.4b* (black dashed line). One standard deviation uncertainty estimates from the bootstrap lie in the order of 3 to 6 degrees for both latitude and longitude and are shown for *CALS3k.4b* as dotted lines in panel a. The VGP reconstructions by Valet et al. (2008) (gray dots) and Nilsson et al. (2010) (version DE-FNBKE, black dots) are also included.

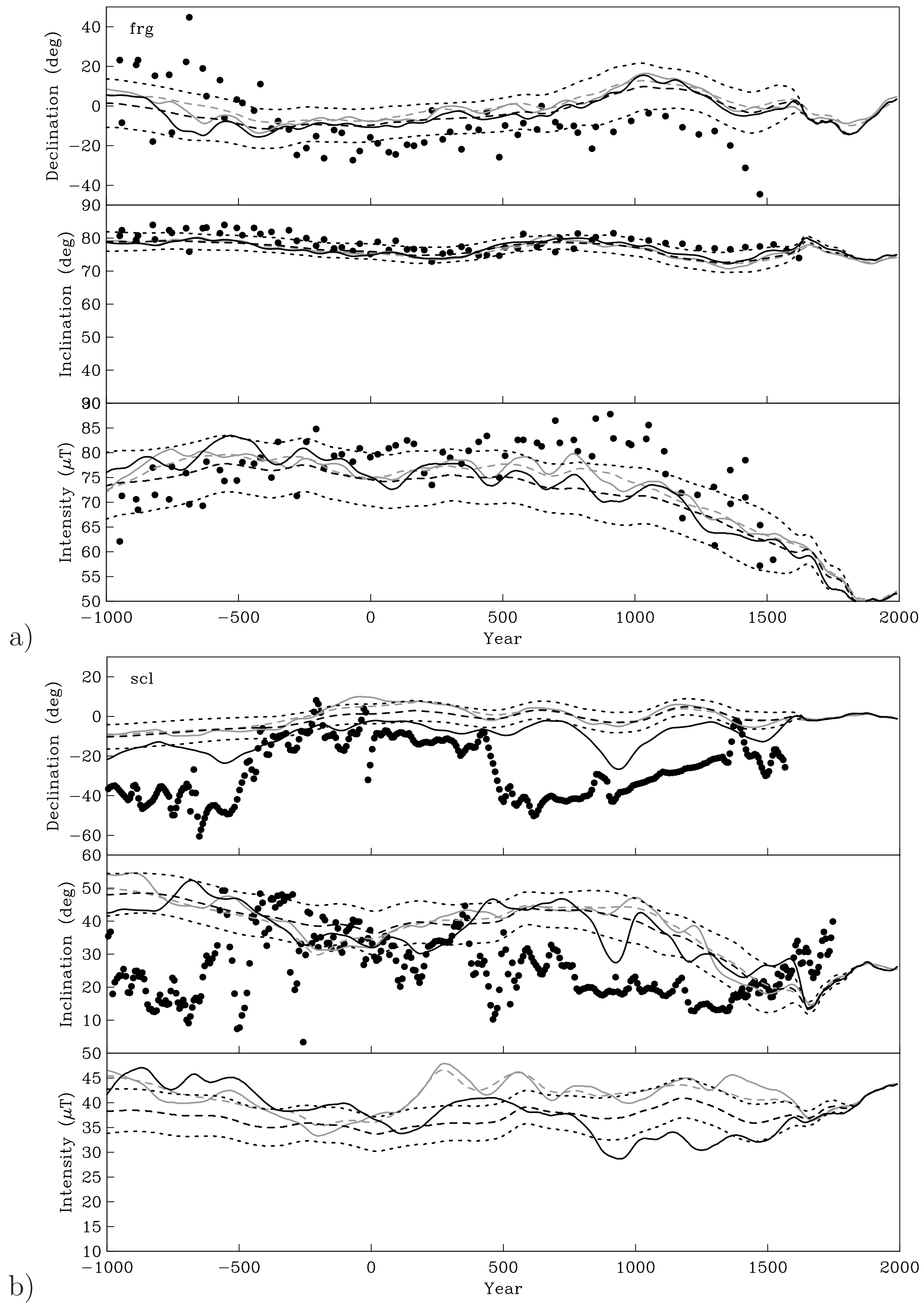

Figure 6: Data (black dots) and predictions of models *CALS3k.3* (gray line), *CALS3k.3b* (dashed gray line), *CALS3k.4* (black line) and *CALS3k.4b* (dashed black line) for lakes a) Frangsjön (Sweden, (Snowball and Sandgren, 2002; Snowball et al., 2007)) and b) Shuangchiling (China, (Yang et al., 2009)). Uncertainty estimates from the bootstrap are of similar magnitude for all models and are shown for *CALS3k.4b* by dotted lines.

to changes in $B_r(c)$ (see for example, Johnson and Constable (1997); Constable (2007)). Figure 7 shows coverage of the core surface via the sum of the absolute value of these linearized data kernels for intensity, inclination, and declination at all available locations. The bottom panel shows kernels for all three elements combined as a sum in commensurate units (with declination and inclination kernels scaled by horizontal and vertical field strength, respectively) for the final *CALS3k.4* data set. Loosely speaking this figure shows the importance of each location on the CMB in contributing to changes in surface observations. We see that the data correspond to a far broader area of coverage at the CMB than is evident from the surface locations in Figure 1. Note that inclination observations respond to lower latitudes on the core surface than the observation site, while declination kernels peak at a longitudinal distance of 23°. Intensity data are critical to determining high latitude field structure. In fact Figure 7 reveals that there is no place on the CMB that does not contribute to changes in the surface observations, although the sensitivity is clearly highest in the middle of the Northern Hemisphere outside the Pacific region.

In Fig. 8 we compare the time-averages of B_r at the CMB for the four models, shown. Differences between (b) and (d), the time-averages of models *CALS3k.3b* and *CALS3k.4b*, are small confirming that the bootstrap average models represent the most robust field features. Although the structures shown by *CALS3k.3* and *CALS3k.4* are also similar, slightly more pronounced differences are seen over the Indonesian-Australian region and in the northern hemisphere flux patches. Animations of the radial field component $\mathrm{B_r}$ at the CMB of all models and of the differences between the individual and averaged models, respectively, are provided as an electronic supplement. Snapshots for two epochs, 400 BC and 500 AD, are shown in Figs. 9 and 10, respectively. Differences between the individual models at some times and for some regions reach $\pm 300\mu$T, that is up to 50% of the radial field strength itself. However, the differences mostly occur in the regions where new data have been added and the overall flux pattern remains broadly similar. For some epochs and regions it seems that structures suggested in *CALS3k.3* are sharpened and more detailed in *CALS3k.4*, but sometimes the centers of flux lobes are shifted significantly between the two models (Figs. 9 and 10 panels a and c). The strongest differences occur over the eastern Siberian / Alaskan region between 1000 BC and 100 BC and again after 500 AD both there and over the Greenland region. Strong differences appear over the South-East-Asian / Australian region nearly all of the time, sometimes also including the Indian Ocean region (Figs. 9 and 10 panels e). Differences between the bootstrap average models are significantly smaller and barely reach $\pm 150\mu$T. They generally appear in similar, but not exactly the same locations as the ones between the individual models. Particularly the differences in the South-East-Asian / Australian region are less pronounced (Figs. 9 and 10 panels f). It is obvious that models *CALS3k.3b* and *CALS3k.4b* are more similar than *CALS3k.3* and *CALS3k.4* and represent more robust estimates of the past field. Interestingly, however, the strongest difference between *CALS3k.3b* and *CALS3k.4b* occurs over the Siberian / Japanese region between 180 AD and 500 AD (see Fig. 10f), at a time when the Siberian difference in the individual models is weaker than most of the time. Between 1640 and 1990 AD strong small-scale differences are seen between both the individual and the averaged models due to the strongly increased agreement with *gufm1*

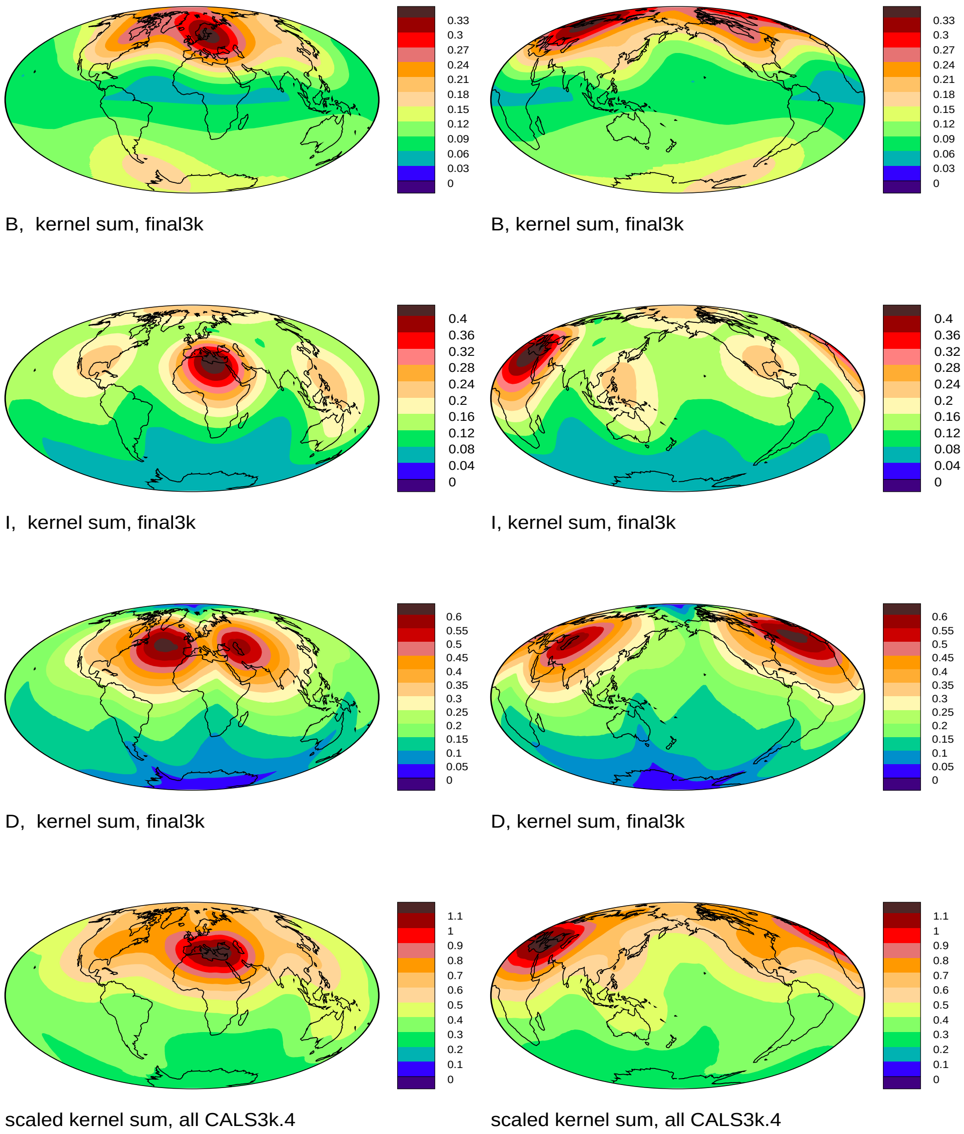

Figure 7: Linearized data kernels for CMB sampling by the time-averaged final data set used to construct *CALS3k.4* and *CALS3k.4b*. For B, I, and D the absolute values are summed for all locations. In the scaled kernel sum of lowermost panels D and I kernels have been scaled by horizontal and vertical field respectively to provide commensurate magnetic field units and combined with B to show global coverage by all data elements (see text for further explanation).

in the version 4 models.

5. Discussion

There are important philosophical differences about how to obtain the most reliable field reconstructions for Holocene time scales, given the large uncertainties in the data. A major problem is that for a significant part of the global data set it is very difficult to get independent, realistic, and internally consistent estimates of the uncertainties. Significant differences in the techniques applied to obtain the data, very different levels of documentation, and the gradual evolution of quality tests that nowadays are considered important but had not been fully developed or routinely applied at the time of older studies aggravate the problem of acquiring consistent estimates for data errors and limit our capabilities for a priori data selection. Stringent data selection following today's state-of-the-art quality criteria significantly reduces global spatial and temporal data coverage. If sediment data are completely rejected the consequence is a strong geographical bias in the data distribution. It is not obvious how to obtain the most reliable past field reconstructions. Our approach has been to include all data (except for the iterative rejection of outliers based on a first guess model) and suppose that the modeling technique will be able to extract statistically consistent signals without being influenced too strongly by incompatible data. Others have limited themselves to high quality archeomagnetic data (Valet et al., 2008) or what can be considered highest quality sediment records (Nilsson et al., 2010) to reconstruct the past evolution of the dipole without considering any smaller scale structure. Incompatible data will result in large misfits to the observations, but so too will any inappropriate restriction of the available structure e.g. by very low degree truncation of spherical harmonic representations.

The apparent sharpening of some field structure of the radial field at the CMB and the increased dipole tilt seen in *CALS3k.4* might be an indication that globally compatible new data have been included and can indeed dominate smoothing effects of incompatible data in our modeling approach. The increased dipole tilts around 600 BC and 1000 AD (Fig. 5) are in good agreement with several recent results including (1) the $\mathrm{DE}_{\mathrm{FNBKE}}$ Virtual Geomagnetic Pole (VGP) model of Nilsson et al. (2010) which is based on five globally distributed sedimentary paleomagnetic records considered to be of highest quality, (2) the purely archeomagnetic VGP model by Valet et al. (2008) and (3) our purely archeomagnetic model *ARCH3k.1* (Korte et al., 2009). The bootstrap averages do not resolve these relatively fast variations and predict much slower movement of the dipole axis with weaker tilt. The westward swing in the dipole axis of *CALS3k.4* around 1300 AD is somewhat similar to the axis behavior predicted by our earlier sediment only model *SED3k.1* (Korte et al., 2009), but contrasts with all other models including the VGP models of Valet et al. (2008) and Nilsson et al. (2010). The fact that the bootstrap average *CALS3k.4b* also fails to support this feature suggests that an eastward swing more accurately describes the past dipole axis behavior at that time.

The comparison of dipole evolution for the un-averaged *CALS3k.3* and *CALS3k.4* models suggests that somewhat higher temporal variability than preserved in the bootstrap av-

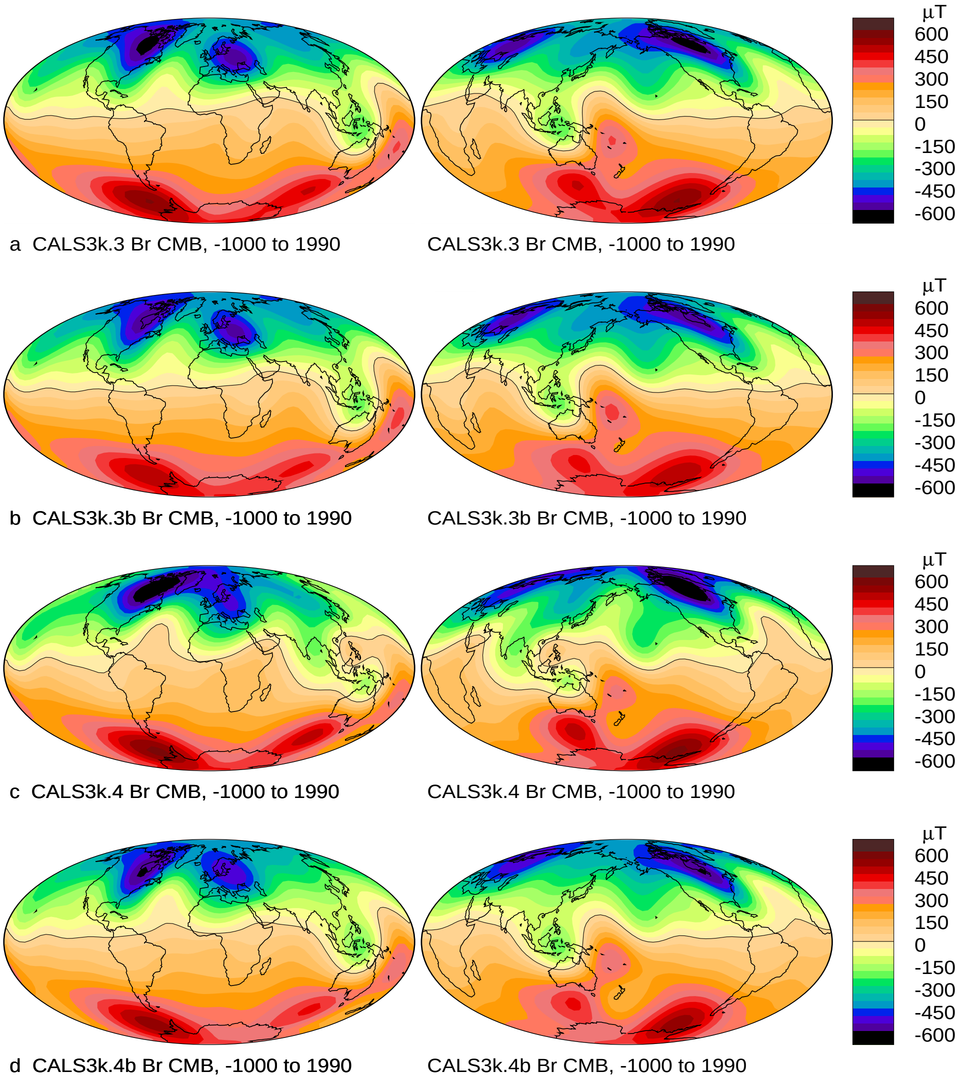

Figure 8: Time-averaged radial field component at the CMB of models a) *CALS3k.3*, b) *CALS3k.3b*, c) *CALS3k.4* and d) *CALS3k.4b* centered on 0° (left) and 180° (right) longitude.

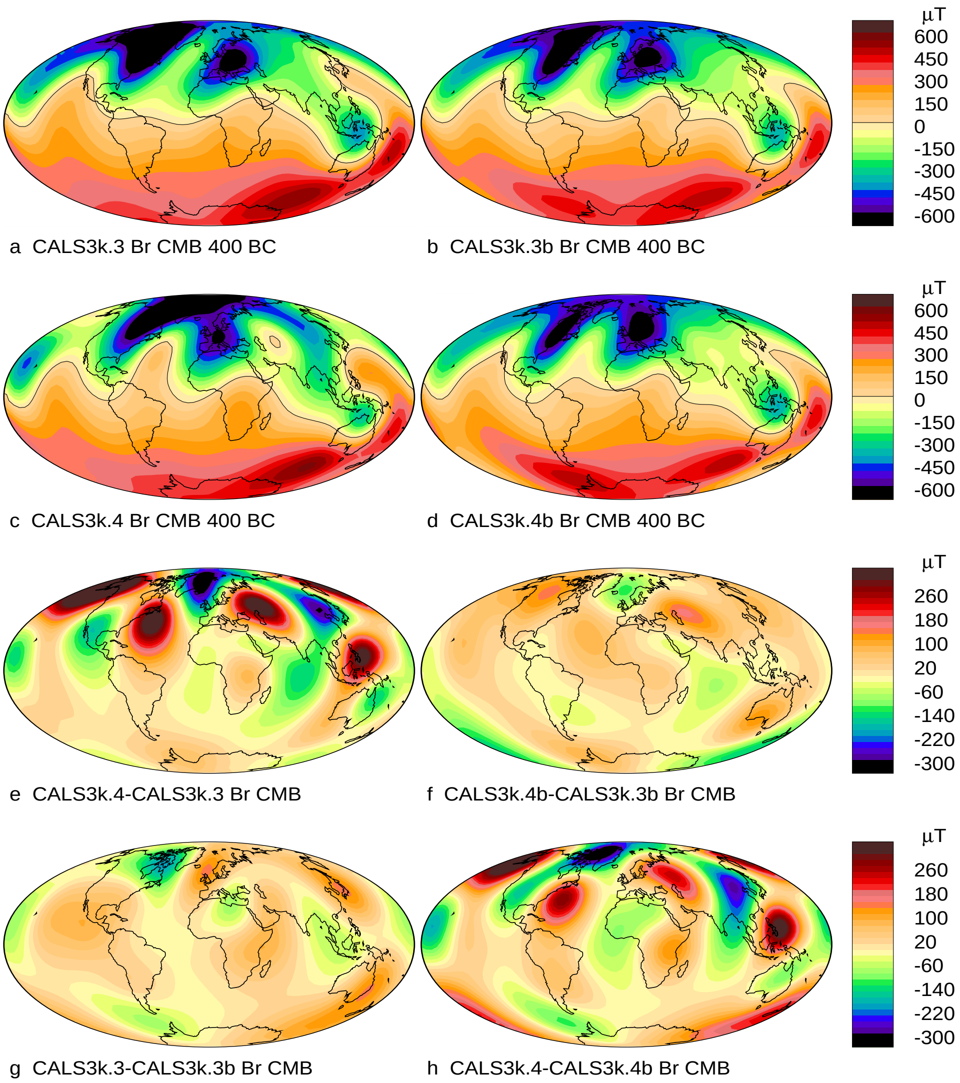

Figure 9: Radial magnetic field at the CMB at epoch 400 BC of models a) *CALS3k.3*, b) *CAL3k.3b*, c) *CALS3k.4* and d) *CALS3k.4b*. Difference between the radial field at the CMB for the same epoch between models (e) *CALS3k.4* and *CALS3k.3*, (f)*CALS3k.4b* and *CALS3k.3b*, (g) *CALS3k.3* and *CALS3k.3b* and (h)*CALS3k.4* and *CALS3k.4b*.

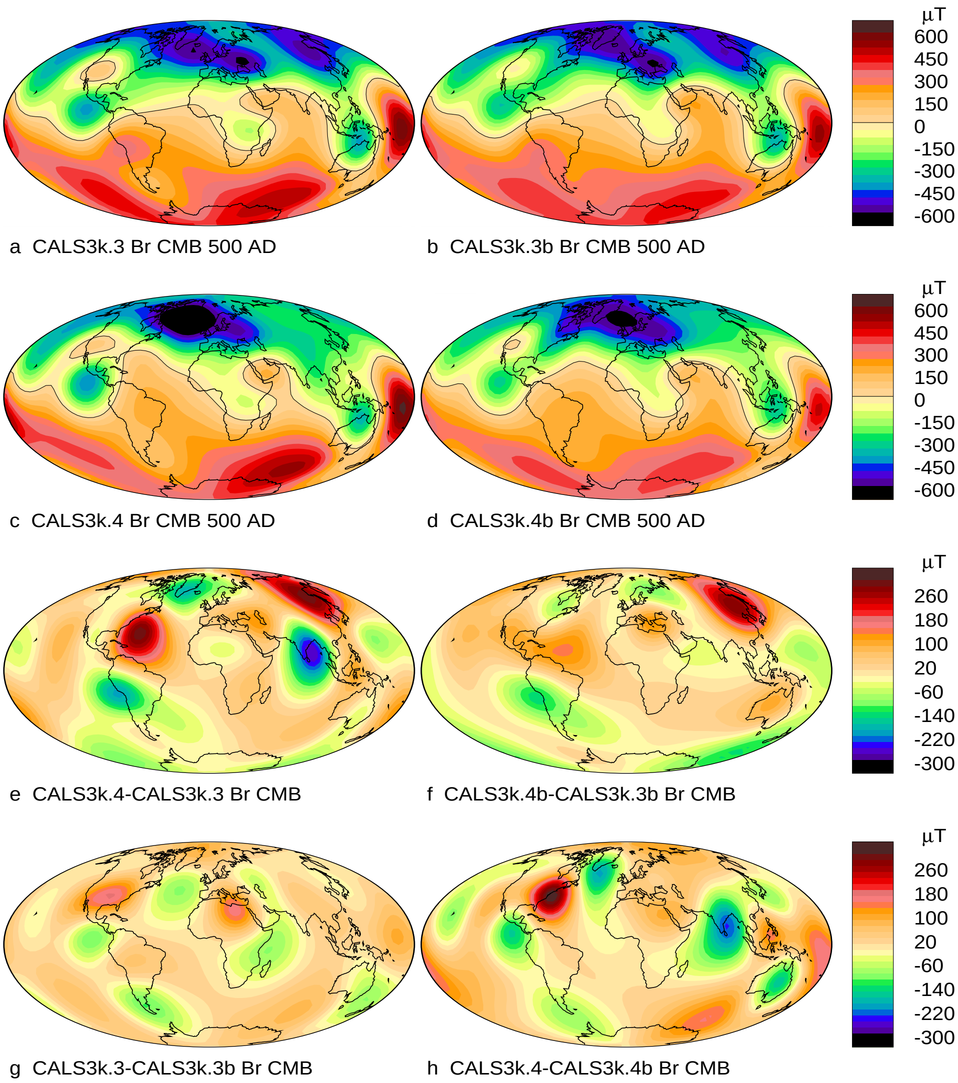

Figure 10: Radial magnetic field at the CMB at epoch 500 AD of models a) *CALS3k.3*, b) *CAL3k.3b*, c) *CALS3k.4* and d) *CALS3k.4b*. Difference between the radial field at the CMB for the same epoch between models *CALS3k.4* and *CALS3k.3* (e), *CALS3k.4b* and *CALS3k.3b* (f),*CALS3k.3* and *CALS3k.3b* (g) and *CALS3k.4* and *CALS3k.4b* (h), respectively.

erages can be resolved. On the other hand, it is surprising how sensitive the general dipole strength is to changes in the data. The lower dipole moment resembles a result that we previously obtained for the exclusively sedimentary *SED3k.1*, and might therefore indicate the growing influence of the increased number of sedimentary data. However, the dipole moment obviously also depends strongly on the calibration of the relative intensity records. The iterative re-calibration of sediment records in *CALS3k.4* is not sufficient to explain the observed discrepancy and it seems surprising that the new model shows a weaker dipole moment than the model that was used to calibrate the relative intensity records. This fact, that the dipole strength of the version 4 models is lower despite the relative intensity records being calibrated by the version 3 model, indicates that the dipole strength is weakly constrained by the intensity data available so far. The regional intensity predictions of the models have not changed much in the regions where intensity data were already available for version 3. The most pronounced differences in field strength predictions are seen in some regions where intensity and directional data are available for the first time in version 4, e.g. up to 20 μT in the Arctic Ocean (sediment record AAM). Further differences in this field component more often appear as offsets in the order of 5 μT rather than changes in variation and in regions devoid of intensity data, e.g. Mexico (record SAN) or Siberia (record LAM). The geomagnetic power spectra suggest that some of the field strength seen as a dipole contribution by *CALS3k.3* has shifted to the octupole contribution in *CALS3k.4* through the influence of the additional data locations. The fact that some of the sedimentary data are fit poorly by all of the models and that several relative intensity records show large standard deviations in the distribution of calibration estimates from any of the models suggest the need for further studies on the global influence of individual data records and their calibrations.

The more detailed comparison of the relatively high resolution individual models *CALS3k.3* and *CALS3k.4* also shows the sensitivity of several model features to changes in the data set in our approach. At Earth's surface, model predictions for times, regions and field components where data contribute to both models are mostly robust, but strong regional differences among the models can occur where that is not the case. The bootstrap averaged models clearly agree more closely in such cases, but at the cost of also showing significantly lower temporal variability for those times and locations where the model is in principle well-constrained by data.

Details of the radial field component at the CMB are also rather sensitive to changes in the data basis. This is not surprising, as a similarly good fit to the data can be achieved by variable distributions of power among different coefficients. The downward continuation to the CMB enhances the small scales, including particularly the noise, and consequently pronounces differences that appear nearly insignificant at the Earth's surface. As we see in Figure 7 the way that the surface observations of different field components sample the field at the CMB can lead to counter-intuitive regional influences of individual data on the model results. Nevertheless, our results generally show the largest differences in the regions where new data have been added. Given the enhancement of small scale features by downward continuation it seems reasonable to prefer the more conservative bootstrap average models for studying geodynamo processes using the evolution of the field at the

CMB .

6. Conclusions

We have presented two updated versions of the *CALS3k* spherical harmonic field model for the past 3kyr using all available archeomagnetic and sediment data. Approximately 5000 new data have been added. In addition to the *CALS3k.4* model based on the individual data compilation, we created average models from bootstrap experiments using data and age uncertainty combined with data distribution for both the old and new versions of the model. This bootstrap averaging to produce *CALS3k.3b* and *CALS3k.4b*, respectively, ensures that only the most robust features of the different models are preserved, while spurious smaller scale (temporal and spatial) structure is averaged out. However, some genuine smaller scale features are also suppressed in this case, which might reflect the need for a more careful evaluation of age uncertainties.

The additional sedimentary records cause notable differences that are mainly in the South-east Asian and Alaskan / eastern Siberian regions according to the geographic distribution of the new data. Somewhat surprisingly, they also have a noticeable effect in lowering the dipole moment prediction of the new model and we plan to investigate the influence of individual sediment records and their calibration further in future work.

Minor improvements of the modeling method include iterative re-calibration of the sedimentary records combined with several iterations of outlier rejection. However, the major differences in the models are caused by changes in the data basis. Another improvement in the version 4 models is a stronger enforcement of the agreement with the *gufm1* model for the historical end of the models. The penalty for departures from *gufm1* was too weak in the *CALS3k.3* model, resulting in artificial field structure in the North American regions after about 1870 AD, produced by end effects from a sediment core at a time when there are hardly any other data from that region.

We have compared several aspects of the individual and bootstrap averaged models and conclude that with the presently available data it is not feasible to produce a model suitable for all possible applications. Our modeling approach uses regularization to produce models tailored for studies of the (large-scale) field evolution at the CMB to investigate geodynamo processes. The more conservative bootstrap average models are better for that purpose as many features in the bootstrap averages proved relatively robust between the old and new versions of the model, while parts of the more detailed structure shown by the individual models might be spurious. For field predictions at the surface, in regions covered by data, the higher resolution individual models are generally robust particularly for the directional data. In regions devoid of data, however, significant differences can be caused by changes in the global data set and again the more conservative bootstrap averages should better represent the general long-term evolution of the field there. Real progress in describing the past field evolution in these areas can only come from new data.

Acknowledgements

We thank Ute Frank for alerting us to newly available sediment records and for useful discussion of paleomagnetic sedimentary data and Fabio Donadini for updating the Geomagia database. Richard Holme provided valuable discussions about the modeling strategy and methods. Two anonymous reviewers provide detailed comments and suggestions for improving the clarity of the manuscript. We wish to express our gratitude to all the colleagues who shared their data with us personally, by making them available as supplemental material with their publications, or by submitting them to databases. Maps were created with programs “magmap” and “color” by Robert Parker. CC acknowledges support from NSF Grant EAR 0809709.

References

Ali, M., Oda, H., Hayashida, A., Takemura, K., Torii, M., 1999. Holocene palaeomagnetic secular variation at Lake Biwa, central Japan. Geophys. J. Int. 136, 218–228.

Barletta, F., St-Onge, G., Channell, J. E. T., Rochon, A., Polyak, L., Darby, D., 2008. High-resolution paleomagnetic secular variation and relative paleointensity records from the western Canadian Arctic: implications for Holocene stratigraphy and geomagnetic field behaviour. Can. J. Earth Sci. 45, 1265–1281.

Bloxham, J., Jackson, A., 1992. Time-dependent mapping of the magnetic field at the core-mantle boundary. J. Geophys. Res. 97, 19,537–19,563.

Brachfeld, S. A., Banerjee, S. K., 2000. A new high-resolution geomagnetic relative paleointensity record for the North American Holocene: A comparison of sedimentary and absolute intensity data. J. Geophys. Res. 105, 821–834.

Chaparro, M. A. E., Böhnel, H. N., Byrne, R., Nowaczyk, N. R., Molina-Garza, R. S., Park, J., Negendank, J. F. W., 2008. Palaeomagnetic secular variation and rock-magnetic studies of Holocene sediments from a maar lake (Hoya de San Nicolas) in Central Mexico. Geophys. J. Int. 175, 462–476.

Constable, C., 2007. Centennial- to millennial-scale geomagnetic field variations. Treatise on Geophysics 4, 337–372.

Constable, C. G., Johnson, C. L., Lund, S. P., 2000. Global geomagnetic field models for the past 3000 years: transient or permanent flux lobes? Phil. Trans. R. Soc. Lond. A 358, 991–1008.

Constable, C. G., Parker, R. L., Stark, P. B., 1993. Geomagnetic field models incorporating frozen-flux constraints. Geophys. J. Int. 113, 419–433.

Donadini, F., Korhonen, K., Riisager, P., Pesonen, L. J., 2006. Database for Holoecene geomagnetic intensity information. EOS Trans. Am. Geophys. Soc. 87(14), 92–93.

Donadini, F., Korte, M., Constable, C., 2009. Geomagnetic field for 0-3ka: 1. new data sets for global modeling. Geochem. Geophys. Geosys. 10, Q06007, doi:10.1029/2008GC002295.

Dumberry, M., Bloxham, J., 2006. Azimuthal flows in the Earth's core and changes in length of day at millennial timescales. Geophys. J. Int. 165, 32–46.

Dumberry, M., Finlay, C. C., 2007. Eastward and westward drift of the Earth's magnetic field for the last three millennia. Earth Planet. Sci. Lett. 254, 146–157.

Frank, U., 2007. Palaeomagnetic investigations on lake sediments from NE China: a new record of geomagnetic secular variations for the last 37 ka. Geophys. J. Int. 169, 29–40.

Gallet, Y., Hulot, G., Chulliat, A., Genevey, A., 2009. Geomagnetic field hemispheric asymmetry and archeomagnetic jerks. Earth Planet. Sci. Lett. 284, 179–186.

Geiss, C. E., Dorale, J. A., Dahms, D., 2007. A rockmagnetic and palaeomagnetic record of two glacial lakes in the Wind River Range, Wyoming, U.S.A. Eos Trans. AGU 88(52), Abstract GP53B–1216.

Genevey, A., Gallet, Y., Constable, C., Korte, M., Hulot, G., 2008. ArcheoInt: An upgraded compilation of geomagnetic field intensity data for the past ten millennia and its application to the recovery of the past dipole moment. Geochem. Geophys. Geosys. 9,Q04038, doi:10.1029/2007GC001881.

Gubbins, D., 1975. Can the Earth's magnetic field be sustained by core oscillations? Geophys. Res. Lett. 2, 409–412.

Haltia-Hovi, E., Nowaczyk, N., Saarinen, T., 2010. Holocene palaeomagnetic secular variation recorded in multiple lake sediment cores from eastern Finland. Geophys. J. Int. 180, 609–622.

Hayashida, A., Ali, M., Kuniko, Y., Kitagawa, H., Torii, M., Takemura, K., 2007. Environmental magnetic record and paleosecular variation data for the last 40 kyrs from the Lake Biwa sediments, Central Japan. Earth Planets Space 59, 807–814.

Hillenbrand, C.-D., Smith, J., Kuhn, G., Esper, O., Gersonde, R., Larter, R., Maher, B., Moreton, S., Shimmield, T., Korte, M., 2009. Age assignment of a diatomaceaous ooze deposited in the western Amundsen Sea Embayment after the last glacial maximum. J. Quater. Sci. 25, 280–295.

Hongre, L., Hulot, G., Khokhlov, A., 1998. An analysis of the geomagnetic field over the past 2000 years. Phys. Earth Planet. Interiors 106, 311–335.

Hyodo, M., Yoshihara, A., Kashiwaya, K., Okimura, T., Matsuzawa, T., Nomura, R., Tanaka, S., Tang, B., Liu, Q., Liu, S., 1999. A late Holocene geomagnetic secular variation record from Erhai Lake, southwest China. Geophys. J. Int. 136, 784–790.

Jackson, A., Jonkers, A. R. T., Walker, M. R., 2000. Four centuries of geomagnetic secular variation from historical records. Phil. Trans. R. Soc. Lond. A 358, 957–990.

Johnson, C., Constable, C., 1998. Persistently anomalous pacific geomagnetic fields. Geophys. Res. Lett. 25, 1011–1014.

Johnson, C. L., Constable, C. G., 1997. The time-averaged geomagnetic field: global and regional biases for 0-5 Ma. Geophys. J. Int. 131, 643–666.

Korhonen, K., Donadini, F., Riisager, P., (2008), L. P., 2008. Geomagia50: an archeointensity database with PHP and MySQL. Geochem., Geophys., Geosys. 9, Q04029, doi:10.1029/2007GC001893.

Korte, M., Constable, C., Donadini, F., 2009. Geomagnetic field for 0-3ka: 2. revised global time-varying models. Geochem. Geophys. Geosys. 10, Q06008, doi:10.1029/2008GC002297.

Korte, M., Constable, C. G., 2003. Continuous global geomagnetic field models for the past 3000 years. Phys. Earth Planet. Interiors 140, 73–89.

Korte, M., Constable, C. G., 2005. Continuous geomagnetic field models for the past 7 millennia: 2. CALS7K. Geochem., Geophys., Geosys. 6, Q02H16, doi:10.1029/2004GC000801.

Korte, M., Constable, C. G., 2006. On the use of calibrated relative paleointensity records to improve millennial-scale geomagnetic field models. Geochem., Geophys., Geosys. 7, Q09004, doi:10.1029/2006GC001368.

Korte, M., Constable, C. G., 2008. Spatial and temporal resolution of millennial scale geomagnetic field models. J. Adv. Space Res. 41, 57–69.

Korte, M., Genevey, A., Constable, C. G., Frank, U., Schnepp, E., 2005. Continuous geomagnetic field models for the past 7 millennia: 1. A new global data compilation. Geochem., Geophys., Geosys. 6, Q02H15, doi:10.1029/2004GC000800.

Kuang, W., Tangborn, A., Jiang, W., Liu, D., Sun, Z., Bloxham, J., Wei, Z., 2008. MoSST_DAS: the first generation geomagnetic data assimilation framework. Comm. Comp. Phys. 3, 85–108.

Lifton, N., Smart, D. F., Shea, M. A., 2008. Scaling time-integrated in situ cosmogenic nuclide production rates using a continuous geomagnetic model. Earth Planet. Sci. Lett. 268, 190–201.

Lisé-Pronovost, A., St-Onge, G., Brachfeld, S., Barletta, F., Darby, D., 2009. Paleomagnetic constraints on the Holocene stratigraphy of the Arctic Alaskan margin. Global and Planetary Change 68, 85–99.

Lodge, A., Holme, R., 2008. Towards a new approach to archaeomagnetic dating in europe using geomagnetic field modelling. Archaeometry 50(3), 309–322.

Maus, S., Macmillan, S., Chernova, T., Choi, S., Dater, D., Golovkov, V., Lesur, V., Lowes, F., Lühr, H., Mai, W., McLean, S., Olsen, N., Rother, M., Sabaka, T., Thomson, A., Zvereva, T., 2005. The 10th generation Internations Geomagnetic Reference Field. Geophys. J. Int. 161, 561–565.

Muscheler, R., Joos, F., Beer, J., Müller, S. A., Vonmoos, M., Snowball, I., 2007. Solar activity during the last 1000yr inferred from radionuclide records. Quat. Sci. Rev. 26, 82–97.

Nilsson, A., Snowball, I., Muscheler, R., 2010. Holocene geocentric dipole tilt model constrained by sedimentary paleomagnetic data. Geochem. Geophys. Geosys. 11,Q08018, doi:10.1029/2010GC003118.

Richter, C., Venuti, A., Verosub, K. L., Wei, K.-Y., 2006. Variations of the geomagnetic field during the Holocene: Relative paleointensity and inclination record from the West Pacific (ODP Hole 1202B). Phys. Earth Planet. Inter. 156, 179–193.

Snowball, I., Sandgren, P., 2002. Geomagnetic field variations in northern Sweden during the Holocene quantified from varved lake sediments and their implications for cosmogenic nuclide production rates. The Holocene 12, 517–530.

Snowball, I., Zillén, L., Ojala, A., Saarinen, T., Sandgren, P., 2007. FENNOSTACK and FENNOPRIS: Varve dated Holocene palaeomagnetic secular variation and relative palaeointensity stacks for Fennoscandia. Earth Planet. Sci. Lett. 255, 106–116.

St-Onge, G., Mulder, T., Piper, D. J. W., Hillaire-Marcel, C., Stoner, J. S., 2004. Earthquake and flood-induced turbidites in the Saguenay Fjord (Québec): a Holocene paleoseimicity record. Quat. Sci. Rev. 23, 283–294.

Stockhausen, H., 1998. Geomagnetic palaeosecular variation (0 - 13 000 yr BP) as recorded in sediments from three maar lakes from the West Eifel (Germany). Geophys. J. Int. 135, 898–910.

Usoskin, I., Korte, M., Kovaltsov, G., 2008. Role of centennial geomagnetic changes in local atmospheric ionization. Geophys. Res. Lett. 35, L05811, doi:10.1029/2007GL033040.

Usoskin, I. G., Solanki, S. K., Korte, M., 2006. Solar activity reconstructed over the last 7000 years: the influence of geomagnetic field changes. Geophys. Res. Lett. 33, L08103, doi:10.1029/2006GL025921.

Valet, J.-P., Herrero-Bervera, E., LeMouël, J.-L., Plenier, G., 2008. Secular variation of the geomagnetic dipole during the past 2000 years. Geochem. Geophys. Geosys. 9, Q01008, doi:10.1029/2007GC001728.

Wardinski, I., Korte, M., 2008. The evolution of the core-surface flow and changes in the length of day over the last seven thousand years. J. Geophys. Res. 113, B05101, doi:10.1029/2007JB005024.

Yang, X., Heller, F., Yang, J., Su, Z., 2009. Paleosecular variations since ∼9000 yr BP as recorded by sediments from maar lake Shuangchiling, Hainan, South China. Earth Planet. Sci. Lett. 288, 1–9.